

Incoming windblown sand drift to civil infrastructures: A probabilistic evaluation

*Original*

Incoming windblown sand drift to civil infrastructures: A probabilistic evaluation / Raffaele, Lorenzo; Bruno, Luca; Fransos, Davide; Pellerey, Franco. - In: JOURNAL OF WIND ENGINEERING AND INDUSTRIAL AERODYNAMICS. - ISSN 0167-6105. - ELETTRONICO. - 166:(2017), pp. 37-47. [10.1016/j.jweia.2017.04.004]

*Availability:*

This version is available at: 11583/2669452 since: 2018-04-17T13:59:59Z

*Publisher:*

Elsevier

*Published*

DOI:10.1016/j.jweia.2017.04.004

*Terms of use:*

This article is made available under terms and conditions as specified in the corresponding bibliographic description in the repository

*Publisher copyright*

Elsevier postprint/Author's Accepted Manuscript

© 2017. This manuscript version is made available under the CC-BY-NC-ND 4.0 license  
<http://creativecommons.org/licenses/by-nc-nd/4.0/>. The final authenticated version is available online at:  
<http://dx.doi.org/10.1016/j.jweia.2017.04.004>

(Article begins on next page)

# Incoming windblown sand drift to civil infrastructures: a probabilistic evaluation

Lorenzo Raffaele<sup>a,d,\*</sup>, Luca Bruno<sup>a,d</sup>, Davide Fransos<sup>b,d</sup>, Franco Pellerey<sup>c</sup>

<sup>a</sup>Politecnico di Torino, Department of Architecture and Design, Viale Mattioli 39, I-10125, Torino, Italy

<sup>b</sup>Optiflow Company, Chemin de la Madrague-Ville 160, F-13015, Marseille, France

<sup>c</sup>Politecnico di Torino, Department of Mathematical Sciences, Corso Duca degli Abruzzi 24, I-10129, Torino, Italy

<sup>d</sup>Windblown Sand Modeling and Mitigation joint research group, Italy-France

---

## Abstract

The accurate prediction of windblown sand drift events approaching human infrastructures and activities is fundamental in arid lands. In both scientific literature and technical practice sand drift estimation is carried out in mean terms. Typically, sand drift net direction and intensity are assessed by means of the resultant drift potential. However, windblown sand suffers a number of epistemic and aleatory uncertainties, related to both the wind and the sand fields. The windblown sand drift estimation in probabilistic terms is useful in the infrastructure design perspective and allows to obtain characteristic values of windblown sand transport. In this study windblown sand is considered as an environmental action in analogy to wind action. Several uncertainties involved in the phenomenon are considered: threshold shear velocity and 10-minute average wind velocity are assumed as random variables. Monte Carlo approach is adopted within a bootstrapping technique in order to assess sand drift in probabilistic terms. The proposed approach is applied to five sites in the Arabian Peninsula. Directional statistics of the sand drift are given for each site.

*Keywords:* windblown sand, drift potential, uncertainty quantification, probabilistic approach, Monte Carlo

---

## Nomenclature

DP	Drift Potential
HW	Hybrid Weibull
MC	Monte Carlo
RDD	Resultant Drift Direction
RDP	Resultant Drift Potential
SD-WA	Sand Deterministic - Wind Averaged
SWP	Sand Wind Probabilistic
$D$	drift potential
$F$	probability distribution function
$F_0$	wind calm rate
$N$	number of occurrences
$Q$	sand transport rate
$R$	resultant drift potential
$T$	reference time
$T_r$	recording time
$U$	wind velocity
$U_{10}$	10-min averaged wind speed

---

\*Corresponding author. Tel: (+39) 011.090.4870. Fax: (+39) 011.090.4999.

Email address: [lorenzo.raffaele@polito.it](mailto:lorenzo.raffaele@polito.it) (Lorenzo Raffaele)

URL: <http://www.polito.it/wsmm> (Lorenzo Raffaele)

<i>c.o.v.</i>	coefficient of variation
<i>d</i>	sand grain diameter
<i>d<sub>r</sub></i>	sand grain reference diameter
<i>f</i>	probability density function
<i>g</i>	gravitational acceleration
<i>k</i>	Weibull shape parameter
<i>p</i>	percentile
<i>sk</i>	skewness
<i>u<sub>*</sub></i>	shear velocity
<i>u<sub>*t</sub></i>	threshold shear velocity
<i>z<sub>0</sub></i>	roughness length
$\Delta t$	sampling interval
$\Delta\theta$	sector width
$\theta$	wind direction
$\lambda$	Weibull scale parameter
$\mu$	mean value
$\rho_a$	air density
$\rho_b$	packed bulk sand density
$\sigma$	standard deviation
#	cardinality
0	calm wind

## 1. Introduction

Windblown sand is of interest for several engineering fields in arid environments (e.g. [Middleton and Sternberg, 2013](#); [Stipho, 1992](#)), from environmental to civil engineering. In particular, windblown sand interacts with a number of civil structures and infrastructures, such as roads (e.g. [Redding and Lord, 1981](#); [Dong et al., 2004](#)), railways (e.g. [Zhang et al., 2007, 2010](#); [Cheng and Xue, 2014](#)), industrial facilities and pipelines (e.g. [Alghamdi and Al-Kahtani, 2005](#)), farms (e.g. [Wang et al., 2010](#)), town and buildings (e.g. [Rizvi, 1989](#); [Bofah and Al-Hinai, 1986](#)). Windblown sand transport results from soil erosion and involves sedimentation around built obstacles. In particular, windblown sand effects on civil structures comprehend, but are not limited to: wind erosion and foundation scouring, moving sand dunes encroaching infrastructures, sand accumulation around structures and infrastructures. Due to the nature of these effects, they can lead to several incremental costs in infrastructure management, e.g. loss of capacity and increased maintenance costs ([Zakeri, 2012](#)), but also to disastrous events, such as train derailment ([Cheng et al., 2015](#)). The design of such infrastructures requires the accurate estimation of the amount of incoming windblown sand that attacks the structure. It significantly vary in space and time. Indeed, on the one hand, line-like infrastructures cross different regions with a wide variety of geomorphological characteristics. On the other hand, infrastructure design must ensure the service life prescribed by standards. Hence, a probabilistic approach to design is necessary to take into account the inborn variability of the phenomenon.

The amount of incoming windblown sand is defined as the mass per unit time and per unit length, and usually called *incoming sand drift*. Phenomenologically, windblown sand is a multi-physics phenomenon which includes wind and sand subfields. Hence, sand drift depends on both the wind velocity and the sand characteristics. The modelling framework to sand drift evaluation has been first introduced by [Fryberger and Dean \(1979\)](#). Their seminal work still grounds the current scientific and technical literature in several application fields, such as fundamental research (e.g. [Al-Awadhi and Al-Awadhi, 2009](#); [Barchyn and Hugenholtz, 2011](#)), geomorphology (e.g. [del Valle et al., 2008](#); [Bogle et al., 2015](#); [Kilibarda and Kilibarda, 2016](#); [Yang et al., 2016](#)), paleo sedimentology (e.g. [Yang et al., 2014](#)), climatology (e.g. [Bogle et al., 2015](#)), coastal management (e.g. [Riksen et al., 2016](#)), civil engineering (e.g. [Dong et al., 2004](#); [Zhang et al., 2010](#); [Cheng et al., 2015](#)). In the [Fryberger and Dean \(1979\)](#) framework, the so-called Drift Potential (DP) is defined for each wind direction, while the Resultant Drift Potential (RDP) and the Resultant Drift Direction (RDD) stand for the magnitude and direction of the vector sum of DP over the directions, respectively. These quantities are called "potential" because they provide a measure of sand-moving capacity of the wind blowing

29 over an ideal sand bed, neglecting the local covering of the ground surface (Pye and Tsoar, 2009). Fryberger and  
 30 Dean (1979) obtain DP per reference time (usually 1 year) by cumulating the sand transport rate  $Q$  over the wind  
 31 speed recording time, and rescaling it on the reference time. In turn,  $Q$  results from the vertical integration of the  
 32 horizontal windblown sand flux. Several semi-empirical models to predict  $Q$  have been proposed so far, reviewed e.g.  
 33 in Dong et al. (2003); Kok et al. (2012); Sherman and Li (2012). Among them, modified Bagnold type models are  
 34 the most widely adopted in literature (see for instance the field studies by Fryberger and Dean, 1979; Al-Awadhi and  
 35 Al-Awadhi, 2009; Barchyn and Hugenholtz, 2011; Sherman and Li, 2012; Sherman et al., 2013; Yang et al., 2014; Liu  
 36 et al., 2015). In particular, the model proposed by Lettau and Lettau (1978) is the most adopted one. They all relate  $Q$   
 37 to the wind shear velocity  $u_*$  and the threshold shear velocity  $u_{*t}$ , that is the shear velocity above which sand transport  
 38 occurs. Usually, such a threshold is assessed as a function of the sand grain diameter  $d$  by means of semi-empirical  
 39 expressions (e.g. Bagnold, 1941; Iversen and White, 1982; Shao and Lu, 2000; McKenna, 2003). According to the  
 40 Authors, it is worth pointing out that the current approach within the Fryberger and Dean (1979) framework is:

- 41 • deterministic with respect to the sand subfield. Indeed, the expressions of the threshold shear velocity  $u_{*t}$  used  
 42 so far are purely deterministic;
- 43 • time-averaged with respect to the wind subfield. The wind speed inborn variability is accounted for, but only  
 44 the mean value of DP is retained because the rescaling on the reference time is tantamount to averaging.

45 Let us call such approach as Sand Deterministic - Wind Averaged (SD-WA).

46 Despite SD-WA approach is generalized in practice, windblown sand phenomenon is affected by several sources  
 47 of uncertainty. They can be generally classified in *aleatory* and *epistemic* uncertainties (Zio and Pedroni, 2013). Let  
 48 us introduce a complementary categorization referring to the wind and sand subfields introduced above. *Epistemic*  
 49 uncertainties are associated with the lack of knowledge about the properties and conditions of the phenomena to be  
 50 modeled. They can be further ascribed to model, parameter and measurement uncertainties. Wind-field epistemic  
 51 uncertainties are generally well quantified, because of its long-standing modelling, while sand-field ones have been  
 52 only recently highlighted with respect to threshold shear velocity (e.g. Barchyn and Hugenholtz, 2011; Raffaele et al.,  
 53 2016) and sand transport rate (e.g. Barchyn et al., 2014). *Aleatory* uncertainties refer to inherent randomness of natural  
 54 phenomena. Let us introduce a further categorization referring to the wind and sand subfields introduced above. Wind-  
 55 related aleatory uncertainties affect the velocity and other environment variables. Sand-related aleatory uncertainties  
 56 take place at both the microscopic scale, i.e. grain irregular shape, grain size distribution, grain relative position on  
 57 the sand bed (e.g. Nickling, 1988; Duan et al., 2013; Edwards and Namikas, 2015), and the macroscopic scale, i.e.  
 58 soil vegetation covering, soil sediment availability, soil moisture and soil crusting (see e.g. McKenna Neuman and  
 59 Nickling, 1989; Lancaster and Baas, 1998; Shao, 2008; Hoonhout and de Vries, 2016). The statistical description of  
 60 wind speed is long-standing and well established, as reviewed e.g. by Carta et al. (2009). Conversely only recently  
 61 the Authors proposed the statistical description of threshold shear velocity (e.g. Raffaele et al., 2016). The cited paper  
 62 substantially contributes to the background of the present study. It includes a comprehensive review on the uncertain-  
 63 ties that affects both experimental measurements and modelling of  $u_{*t}$ . In the light of this, a statistical modelling is  
 64 developed, based on advanced copula-based quantile regression. Joint probability density functions of the sand grain  
 65 diameter and  $u_{*t}$  are derived, as well as the conditional probability density functions of the threshold shear velocity  
 66 for given values of the diameter.

67 Both the engineering design needs and the shortcomings of the SD-WA approach pave the way for the proba-  
 68 bilistic description of the incoming sand drift. According to the Authors, it can be regarded as equivalent to other  
 69 environmental actions, in analogy to wind action. Hence, let us briefly outline in the following to which extent the  
 70 incoming wind speed  $U$  is analogous to the sand transport rate  $Q$  and to the drift potential DP. First, in wind engi-  
 71 neering the wind speed is defined in probabilistic terms due to the uncertainty related to inborn wind variability only.  
 72 The probabilistic representation of sand transport rate is recommended a fortiori and it is more difficult at the same  
 73 time, since it is affected by more uncertainties. The variability of both wind and sand features should be taken into  
 74 account. Second, most of the wind effects on structures, e.g. equivalent static loads or flutter, are related to extreme  
 75 values of the incoming wind speed. Conversely, windblown sand effects on civil structures are mainly induced by the  
 76 cumulated values of current values of  $Q$  over time, that is DP. In this perspective, windblown sand effects and related  
 77 assessment recall wind-induced fatigue. In spite of this analogy, some differences remain. Only a few incoming wind  
 78 directions are considered in directional wind-induced fatigue assessment (see e.g. Repetto and Solari, 2004), i.e. the

ones that induce the highest stresses on the cross section. Conversely, all incoming wind directions are taken into account in assessing the windblown sand drift, since they all contribute in RDP definition.

Bearing the above analogy in mind, three main questions may rise to the Authors' mind: i. How does the uncertainty of both threshold shear velocity and mean wind velocity jointly propagate to RDP? ii. Does the probability distribution of RDP change significantly from a site to another in the same region? iii. Does the gap between characteristic and mean value of RDP make the approach of interest for engineering practice?

The present study aims at contributing in shedding some light on such issues. A general probabilistic approach is proposed and applied to real world sites in Arabian Peninsula. Each site is characterized by its actual wind field and sand granulometry. In particular, variability of both sand characteristics at microscopic scale (comprehensively reflected by threshold shear velocity) and wind speed (i.e. wind direction and intensity) are considered. Other sources of uncertainties reviewed above are not included because the lack of their statistical description. As a result, instead of a single pair of values describing mean RDP magnitude and direction, their probability distributions are obtained. Characteristic values are derived from them, and design values can be derived in turn towards a semi-probabilistic approach. The paper develops accordingly to the above objectives through the following sections. In Section 2, the proposed probabilistic approach is outlined. In Section 3, results referred to some chosen Sites in Arabian Peninsula are shown, compared and discussed. In Section 4, conclusions and perspectives are outlined.

## 2. Methods

In the following, the proposed probabilistic approach based on the general framework of Fryberger and Dean (1979) is outlined. First, the framework proposed by Fryberger and Dean (1979) is recalled. Then, the proposed probabilistic approach to assess sand drift is shown step-by-step.

Fryberger and Dean (1979) define the directional drift potential and the resultant drift potential on the basis of the model proposed by Lettau and Lettau (1978), where the sand transport rate  $Q_\theta$  in a given direction  $\theta$  is expressed as

$$\begin{aligned} Q_\theta &= 6.7 \sqrt{\frac{d}{d_r}} \frac{\rho_a}{g} u_{*,\theta}^3 \left(1 - \frac{u_{*t}}{u_{*,\theta}}\right) & \text{if } u_{*,\theta} > u_{*t} \\ Q_\theta &= 0 & \text{if } u_{*,\theta} \leq u_{*t}, \end{aligned} \quad (1)$$

being  $d$  the sand grain diameter,  $d_r = 0.25 \text{ mm}$  the reference sand grain diameter,  $\rho_a$  the air density,  $g$  the gravitational acceleration,  $u_{*t}$  the threshold shear velocity and  $u_{*,\theta}$  the shear velocity in the corresponding wind direction.

The directional drift potential  $D_\theta$  (i.e. DP in Fryberger and Dean, 1979, notation) is rephrased as

$$D_\theta = \frac{1}{\rho_b} \frac{T}{T_r} \sum_{i=1}^{N_\theta} Q_{\theta,i} \Delta t = \frac{T}{T_r} \sum_{i=1}^{N_\theta} D_{\theta,\Delta t,i} \quad (\text{or } D_\theta = 0 \text{ if } N_\theta = 0), \quad (2)$$

where  $\rho_b$  is the packed bulk sand density,  $T$  is the reference time and  $T_r$  is the recording time set as a multiple of  $T$ .  $\Delta t$  is the sampling interval of the wind speed, not necessarily equal to the 10-minute averaging time, for the sake of generality. The drift potential over the sampling interval  $D_{\theta,\Delta t}$  [ $m^3 m^{-1} \Delta t^{-1}$ ] is estimated postulating  $Q_\theta$  [ $Kg m^{-1} s^{-1}$ ] constant over  $\Delta t$ .

$N_\theta$  follows as the number of occurrences in the reference time in which the wind will blow in the direction  $\theta$ , and it is expressed as

$$N_\theta = \frac{T}{T_r} \frac{T_\theta}{\Delta t}, \quad \text{constrained by} \quad \sum_{\theta=1}^{2\pi/\Delta\theta} N_\theta + N_0 = N, \quad (3)$$

where  $T_\theta$  is the time over which the wind blows in the direction  $\theta$ ,  $\Delta\theta$  is the sector width on which the wind is recorded,  $N_0$  and  $N$  are the number of occurrences of calm wind and the number of total occurrences in the reference time  $T$ , respectively.

Finally, the resultant drift potential  $R$  (i.e. RDP in Fryberger and Dean, 1979, notation) can be easily obtained from the vector sum of  $D_\theta$ :

$$R = \sum_{\theta=1}^{2\pi/\Delta\theta} D_\theta. \quad (4)$$

115 In the following, resultant drift potential magnitude and direction are defined as  $|R|$  and  $\hat{R}$ , respectively.  
 116 It may be useful to highlight that Fryberger and Dean (1979) provide also an index of the directional variability of  
 117 windblown sand drift, i.e. the ratio between the resultant drift potential magnitude and the sum of drift potential  
 118 modulus:

$$R/D = \frac{|R|}{\sum_{\theta=1}^{2\pi/\Delta\theta} |D_{\theta}|}. \quad (5)$$

119 In particular, the lower the ratio, the higher the directional variability.

120 In the proposed probabilistic approach the input quantities  $u_{*t}$  and  $u_{*,\theta}$  are random variables. Hence, the Fryberger  
 121 and Dean (1979) framework has to be adapted in order to deal with such random variables. Let us call such approach  
 122 as Sand Wind Probabilistic (SWP). The steps followed in SWP approach are sketched in the flow chart in Figure 1  
 and described in the following.

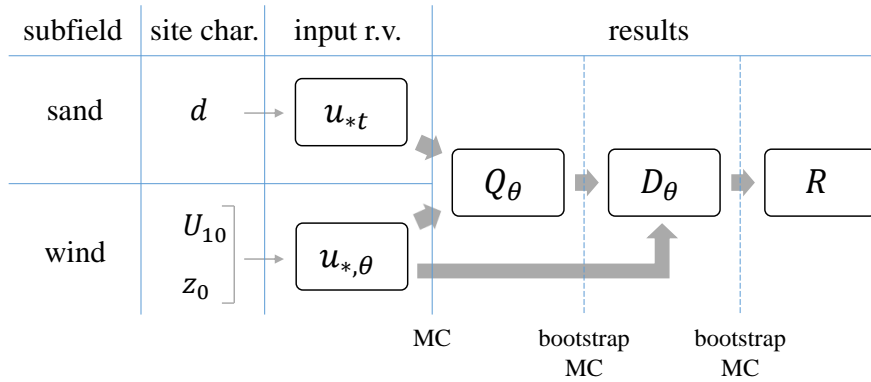


Figure 1: Flow chart of the proposed SWP approach

123 The site characteristics are needed as input data, with respect to both sand subfield (mean sand diameter  $d$ ) and  
 124 wind subfield (aerodynamic roughness  $z_0$  and time series of 10-minute averaged wind speed  $U_{10}(t)$ ). The input ran-  
 125 dom variables  $u_{*t}$  and  $u_{*,\theta}$  are described from the probability density functions  $f(u_{*t})$  and  $f(u_{*,\theta})$ , respectively. To the  
 126 Authors' best knowledge, there are no experimental evidence or systematic studies in literature about a dependence  
 127 between  $u_{*,\theta}$  and  $u_{*t}$ . In this study, the directional shear velocity and the threshold shear velocity are considered in-  
 128 dependent random variables. Indeed,  $u_{*t}$  depends entirely on the sand characteristics, while  $u_{*,\theta}$  depends only on the  
 129 wind velocity for a given  $z_0$ .  $f(u_{*,\theta})$  is simply obtained by rescaling the probability density function  $f(U_{10,\theta})$ , being  
 130  $u_{*,\theta} = 0.41U_{10,\theta}/\ln(z/z_0)$ . Hence, Weibull-type  $f(u_{*,\theta})$  results. The conditional probability density functions  $f(u_{*t} | d)$   
 131 are obtained in Raffaele et al. (2016). Interested readers can refer to the paper above for further details. Here, Figure  
 132 2 is limited to summarize the final finding of that study, i.e. the statistical description of the threshold shear velocity  
 133 versus mean sand diameter  $d$  by means of some percentiles and statistical moments: the mean value  $\mu(u_{*t})$  and 1<sup>st</sup>,  
 134 5<sup>th</sup>, 25<sup>th</sup>, 75<sup>th</sup>, 95<sup>th</sup> and 99<sup>th</sup> percentiles  $p(u_{*t})$ .

136 The sand transport rate model proposed by Lettau and Lettau (1978) is adopted because it is widespread in scien-  
 137 tific and technical literature (e.g. Fryberger and Dean, 1979; Al-Awadhi and Al-Awadhi, 2009; Barchyn and Hugen-  
 138 holtz, 2011; Yang et al., 2014; Liu et al., 2015), and judged performing better than other sand transport models  
 139 (Sherman et al., 2013).  $Q_{\theta}$  results from the transformation of the continuous random variables  $u_{*,\theta}$  and  $u_{*t}$ .  $Q_{\theta}$  is  
 140 expected to be a mixed random variable. In fact,  $Q_{\theta}$  is characterized by a discrete part, i.e.  $Q_{\theta} = 0$ , and a continuous  
 141 part, i.e.  $Q_{\theta} > 0$ , because of the nature of the adopted sand transport rate model (Eq. 1).  
 142 Analytically, given the independent random variables  $u_{*,\theta}$  and  $u_{*t}$ , the probability density function  $f(Q_{\theta})$  for a given  
 143 value of  $d$  can be evaluated by differentiating its distribution function  $F(Q_{\theta})$ , which, for  $q \geq 0$  and  $u_{*,\theta} > u_{*t}$ , can be

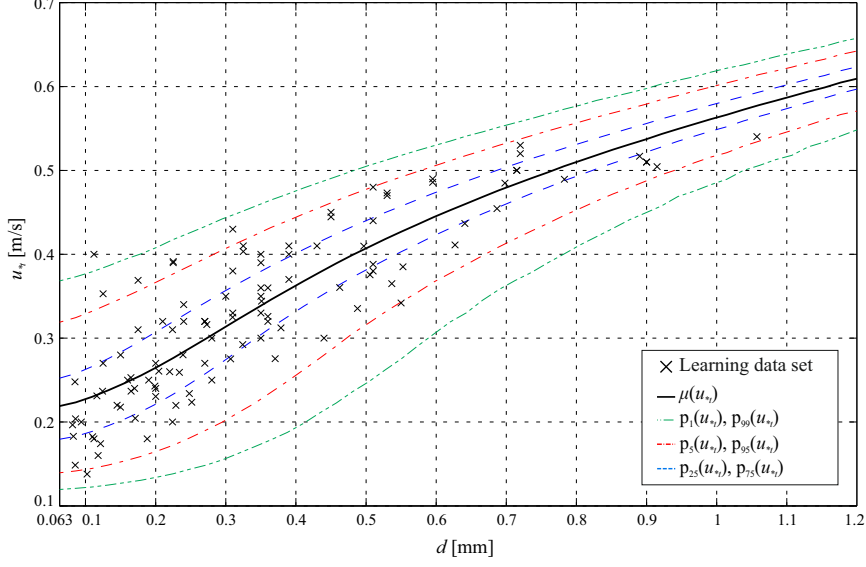


Figure 2: Threshold shear velocity statistics. Mean values  $\mu(u_{*t})$  and percentiles  $p_1(u_{*t})$ ,  $p_5(u_{*t})$ ,  $p_{25}(u_{*t})$ ,  $p_{75}(u_{*t})$ ,  $p_{95}(u_{*t})$ ,  $p_{99}(u_{*t})$

144 expressed as

$$\begin{aligned}
 F_{Q_\theta}(q) &= P[Q_\theta \leq q] = P\left[\left\{6.7 \sqrt{\frac{d}{d_r}} \frac{\rho_a}{g} u_{*,\theta}^3 \left(1 - \frac{u_{*t}}{u_{*,\theta}}\right) \leq q\right\} \cap \{u_{*,\theta} > u_{*t}\}\right] \\
 &= \int \int_{\{(v_1, v_2) : v_1 > v_2; v_1^3 \left(1 - \frac{v_2}{v_1}\right) \leq \frac{q}{6.7} \sqrt{\frac{d_r}{d}} \frac{g}{\rho_a}\}} f_{(u_{*,\theta}, u_{*t})}(v_1, v_2) dv_1 dv_2 \\
 &= \int_0^\infty \left[ \int_{v_1 - \frac{1}{v_1^2} \frac{q}{6.7} \sqrt{\frac{d_r}{d}} \frac{g}{\rho_a}}^{v_1} f_{(u_{*,\theta}, u_{*t})}(v_1, v_2) dv_2 \right] dv_1 \\
 &= \int_0^\infty \left( F_{u_{*t}}(v_1) - F_{u_{*t}}\left(v_1 - \frac{1}{v_1^2} \frac{q}{6.7} \sqrt{\frac{d_r}{d}} \frac{g}{\rho_a}\right) \right) f_{u_{*,\theta}}(v_1) dv_1.
 \end{aligned} \tag{6}$$

145 However, apart for the untractable analytical solution of this double integration,  $f(Q_\theta)$  cannot be expressed in explicit  
 146 form because  $f(u_{*t} | d)$  is given by a non-parametric kernel density function (Raffaele et al., 2016).

147 Numerically, Monte Carlo (MC) simulations can be applied (Caffisch, 1998). This approach presents three substantial  
 148 advantages. First, MC convergence is independent from the number of random variables involved. In fact, it converges  
 149 with a rate equal to  $1/\sqrt{m}$ , where  $m$  is the number of realizations, regardless of the number to random variables.  
 150 Second, the very low cost of each single numerical realization of  $Q_\theta$  allows to perform a large number of realizations  
 151 for each wind direction. Finally, MC allows to describe the mixed random variable  $Q_\theta$  in a straightforward manner.

152 It is worth pointing out that  $N_\theta$  (Eq. 3) is a random quantity because  $T_\theta$  is. For this reason, the probability  
 153 distribution of the directional drift potential  $g(D_\theta)$  should be expressed as a mixture of convolutions

$$g(D_\theta) = \sum_{n=1}^{\infty} (f_1 * \dots * f_i * \dots * f_n)(D_{\theta,\Delta t}) P[N_\theta = n] \quad \text{with} \quad f_i = f \quad \text{for} \quad i = 1, \dots, N_\theta, \tag{7}$$

154 whose corresponding mean  $\mu$  and variance  $\sigma^2$  are

$$\begin{aligned}
 \mu(D_\theta) &= \mu(N_\theta) \mu(D_{\theta,\Delta t}) \\
 \sigma^2(D_\theta) &= \mu(N_\theta) \sigma^2(D_{\theta,\Delta t}) + \mu^2(D_{\theta,\Delta t}) \sigma^2(N_\theta).
 \end{aligned} \tag{8}$$

155 In particular, the variance results from the sum of two terms, the first due to the variance of  $D_{\theta,\Delta t}$  and the second  
 156 to the variance of  $N_{\theta}$ . It should be pointed out that adoption of a non-random  $N_{\theta}$  implies an underestimation of  
 157 the uncertainty of  $D_{\theta}$ , being in this case  $\sigma^2(N_{\theta}) = 0$ . It should be also observed that the constraint on the whole  
 158 set  $\{N_{\theta}, \theta = 1, 2, \dots, n\}$  (see Eq. 3) induces a negative dependence between the variables  $N_{\theta}$ , and consequently in  
 159 the set  $\{D_{\theta}, \theta = 1, 2, \dots, n\}$ , which plays a key role in the final distribution of  $R$ . Unfortunately, the description of  
 160 such an effect of the dependence between the variables  $N_{\theta}$  can not be provided in a simple and tractable analytical  
 161 manner. For these reasons, a Monte Carlo approach, based on bootstrapping techniques (Efron and Tibshirani, 1993)  
 162 from the data set of observed values to generate samples, has been adopted. For each simulation, first the vector  
 163  $N = (N_1, N_2, \dots, N_n)$  of registered occurrences of wind in the considered directions has been obtained from the data  
 164 set. Then, for each direction  $\{\theta = 1, 2, \dots, n\}$ , a sample of cardinality  $N_{\theta}$  of realizations of  $D_{\theta,\Delta t}$  has been randomly  
 165 chosen. Finally, the matrix  $\mathbf{D} = (D_1, D_2, \dots, D_n)$  has been simulated through

$$\mathbf{D} = \begin{bmatrix} D_1 \\ D_2 \\ \vdots \\ D_{\theta} \\ \vdots \\ D_n \end{bmatrix} = \begin{bmatrix} \sum_{i=1}^{N_1} D_{1,\Delta t,i} \\ \sum_{i=1}^{N_2} D_{2,\Delta t,i} \\ \vdots \\ \sum_{i=1}^{N_{\theta}} D_{\theta,\Delta t,i} \\ \vdots \\ \sum_{i=1}^{N_n} D_{n,\Delta t,i} \end{bmatrix}, \quad (9)$$

166 where any  $D_{\theta,\Delta t,i}$  is a realization of  $D_{\theta,\Delta t}$  previously extracted from the data set.

167 Analytically,  $R$  is the vector sum of the components  $D_{\theta}$  of the matrix  $\mathbf{D}$  (Eq. 4), thus a realization of the resultant  
 168 drift potential  $R$  can be immediately assessed once the realization of  $\mathbf{D}$  is given. A set of numerical realizations of  $R$   
 169 can be computed by repeating the same procedure multiple times, and the distribution of  $R$  can be estimated through  
 170 such a sample.

### 171 3. Applications and results

172 In the following, the proposed SWP approach is applied to five Sites located in the Arabian Peninsula. In Sub-  
 173 section 3.1, the layout of the study is shown. Geographical location and aeolian sand grain size of the chosen sites  
 174 are reported. In Subsection 3.2, SWP approach is applied to Site 1. Obtained results are shown in terms of both  
 175 intermediate, i.e.  $Q_{\theta}$  and  $D_{\theta}$ , and final, i.e.  $R$ , results in order to follow and comment step-by-step the full adopted  
 176 procedure. Finally, in Subsection 3.3, final results from Sites 1-5 sites are summarized and compared.

#### 177 3.1. Study layout

178 The site selection obeys to three criteria. Sites with a complete enough anemometric database are first retained.  
 179 Among them, sites are selected to sample the huge variability of both sand and wind subfields in Arabian Peninsula.  
 180 Finally, sites are chosen in reason of their proximity to railway lines having in mind the vulnerability of such infras-  
 181 tructures to windblown sand.

182 In Figure 3, Sites 1-5 are represented on Arabian Peninsula (blue dots). On the same Figure, some operating/under  
 183 construction/planned railway tracks are sketched. In particular, the 950 km long Saudi Landbridge links Jeddah with  
 184 the Saudi Arabia capital Riyadh. The 2750 km North South Railway Line links northern Saudi Arabia with Riyadh  
 185 and the port city Ras Al-Khair. The 450 km long Haramain High Speed Rail links the cities of Medina and Mecca.  
 186 Ethiad Rail is part of the United Arab Emirates' national 1200 km railway network.

187 Sites coordinates and mean sand grain size  $d$  are reported in Table 1. Mean grain sizes are derived from sedimentology  
 188 studies of arabian sand dunes (Al-Sari and Uddin, 1981; Ehlen, 1993; Al-Harhi, 2002; Edgell, 2006). In particular,  
 189 Sites 1, 3 and 4 are sensitive to the sand of Ad Dahna desert, made of medium grained, well sorted quartz sand. Site 2  
 190 is sensitive to the sand of Jeddah plain. Site 5 is sensitive to the fine grained, moderately well sorted sand of Rub' al  
 191 Khali desert.

192 The aerodynamic roughness is set equal to  $z_0 = 4e-3$  m in all Sites. The wind velocity dataset refers to  $T_r = 5$   
 193 years from January 2008 to December 2012 for all stations as well. The 10-min average wind direction is measured  
 194 in the horizontal plane with a sampling interval  $\Delta\theta = 10^\circ$  at all the selected anemometric stations.  $n = 36$  directions

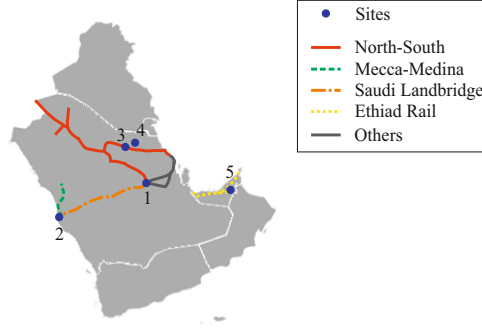


Figure 3: Sketch of the selected sites (blue dots) and railways tracks (lines)

Table 1: Sites of incoming sand drift estimation

Site number	Site name	Latitude	Longitude	$d$ [mm]
1	Riyad	24°4'1.20"N	47°34'58.80"E	0.35
2	Jeddah	21°41'60.00"N	39°10'58.80"E	0.25
3	Hafr Al-Batin	27°55'1.20"N	45°31'1.20"E	0.30
4	Al Qaisumah	28°19'1.20"N	46°7'58.80"E	0.30
5	Al Ain	24°12'2.99"N	55°45'40.00"E	0.16

195 result. The 10-min average wind velocity is recorded with a sampling interval in time  $\Delta t = 1$  hour at all the anemo-  
 196 metric stations (sampling rate 24/144). The actually available datasets at the selected anemometric stations include  
 197 missing data due to anemometric breakdowns and/or operational problems. Missing data are in average equal to 4%  
 198 of the complete dataset. They are evaluated to be almost uniformly distributed along the day. Both the sampling rate  
 199 and missing data are sources of incompleteness of the dataset. In literature (see e.g. Burlando et al., 2013) is widely  
 200 accepted that randomly distributed data incompleteness is usually not influential on the probability distribution of the  
 201 10-min average wind velocity, while it may lead to underestimations of the extreme values. It is worth recalling that  
 202 windblown sand drift potential  $R$  is mainly induced by the cumulated values of current values of  $Q$  over time, result-  
 203 ing from the 10-min average wind velocity in turn. Hence, data incompleteness is not expected to affect the obtained  
 204 results. Finally, the resultant drift potential  $R$  is expressed over a reference time  $T = 1$  year.

205 The results discussed in the next Subsections are obtained by MC approach. Hence, results convergence should be  
 206 discussed every time a random variable is introduced and numerically generated. Convergence is classically evaluated  
 207 by referring to weighted residuals of the first statistical moments of each random variable. The cardinality of the set  
 208 of realizations for each random variable is chosen in order to reach a weighted residual lower or at least equal to  $1e-2$ .  
 209 In the following, the cardinality of each random variable is reported for the sake of completeness, while convergence  
 210 studies are not reported for the sake of brevity.

### 211 3.2. Results for site 1

212 The characteristics of the in-situ sand subfield is summarized by  $d = 0.35$  mm (Table 1). The related input random  
 213 variable is the threshold shear velocity. Its probability density function  $f(u_{*t}|d = 0.35 \text{ mm})$  is derived from Raffaele  
 214 et al. (2016). Related  $u_{*t}$  statistics are reported in Table 2 in terms of mean value  $\mu$ , standard deviation  $\sigma$  and coefficient  
 215 of variation *c.o.v.* It is worth recalling that  $f(u_{*t}|d)$  is the same in each wind direction, since it depends solely on sand  
 216 characteristics.

217 The wind subfield is obtained by mean wind speed in-situ measurements.  $U_{10}$  variability is assessed in terms of both  
 218 *non-directional* and *directional* statistics.

219 *Non-directional* statistics is summarized in Figure 4.  $U_{10}$  time history is shown in Figure 4(a). Both mean wind speed

220  $\mu(U_{10})$  and mean threshold velocity  $\mu(U_t)$  are plotted on the same graph.  $U_{10}$  variability is described by the Hybrid  
 221 Weibull (HW) model (Takle and Brown, 1978). HW probability density function  $f(U_{10})$  is defined as follows:

$$f_{(\lambda,k)}(U_{10}) = \begin{cases} F_0 & \text{for } U_{10} = 0 \\ (1 - F_0) \frac{k}{\lambda} \left(\frac{U_{10}}{\lambda}\right)^{k-1} e^{-U_{10}/\lambda^k} & \text{for } U_{10} > 0 \end{cases} \quad (10)$$

222 where  $F_0$  is the rate of zero values, i.e. the frequency of calm wind,  $k$  is the shape parameter and  $\lambda$  is the scale  
 parameter. HW  $f(U_{10})$  is plotted in Figure 4(b).

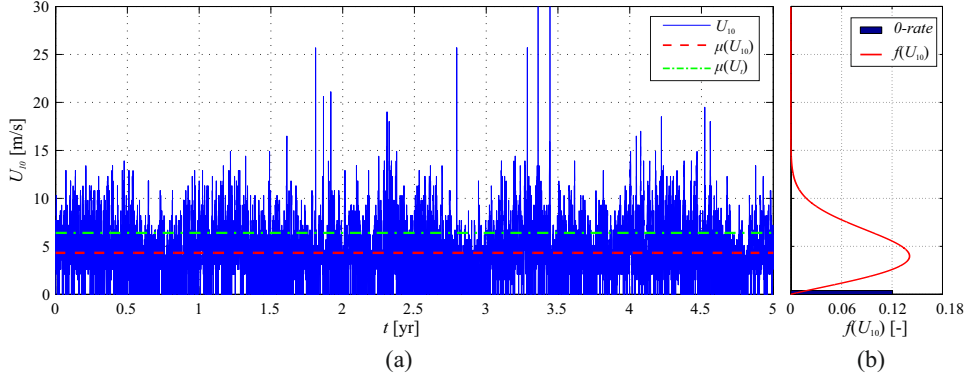


Figure 4: Site 1. Non-directional statistics of mean wind speed: Wind time history (a) and Hybrid Weibull fitting (b)

223 Wind shear velocity is recovered from mean wind speed in-situ measurement. HW  $f(U_{10})$  is rescaled into HW  $f(u_*)$ .  
 224  $u_*$  statistical parameters and moments are reported in Table 2, where they can be compared with  $u_{*t}$  ones. In particular,  
 225 the threshold shear velocity is higher than the shear velocity in mean terms, while the highest variability is addressed  
 226 to the wind subfield.

Table 2: Site 1. Statistical parameters and moments of the non-parametric  $f(u_{*t}|d = 0.35 \text{ mm})$  and Hybrid Weibull  $f(u_*)$

Random variable	$F_0$ [-]	$k$ [-]	$\lambda$ [ $m \text{ s}^{-1}$ ]	$\mu$ [ $m \text{ s}^{-1}$ ]	$\sigma$ [ $m \text{ s}^{-1}$ ]	<i>c.o.v.</i> [-]
$u_{*t}$	-	-	-	0.34	0.06	0.18
$u_*$	0.12	2.09	0.29	0.25	0.13	0.50

227 *Directional* statistics is shown by means of the wind rose and the polar diagram in Figure 5. Calm wind, i.e.  $U_{10,\theta}$   
 228 null values, is filtered since it is non-directional by nature and does not contribute in defining directional statistics.  
 229 Figure 5(a) shows a very broad wind directionality. However, North and South-SouthEast are the directions having  
 230 the highest occurrence frequency. In Figure 5(b), the empirical probability density function of the wind speed in  
 231 North direction is shown as an example. Figure 5(c) depicts the variation of probability density function of both wind  
 232 speed  $U_{10,\theta}$  and erosion threshold  $U_t$  by means of their directional mean values values and extreme percentiles (i.e.  
 233  $5^{th}$  percentile  $p_5$  and  $95^{th}$  percentile  $p_{95}$ ), as a function of wind direction  $\theta = 1, \dots, n$ .  $\mu(U_t)$  is higher than  $\mu(U_{10,\theta})$   
 234 for every direction, but the  $95^{th}$  percentile of the wind speed  $p_{95}(U_{10,\theta})$  overcomes the corresponding percentile of the  
 235 threshold velocity  $p_{95}(U_t)$  for winds blowing from around North and from South-SouthWest.  
 236

237  $U_{10,\theta}$  is converted into  $u_{*,\theta}$  dataset. Classic Weibull probability density function  $f(u_{*,\theta})$  are fitted for each direction.  
 238 Numerical realizations of  $u_{*t}$  and  $u_{*,\theta}$ , consistent with  $f(u_{*t})$  and  $f(u_{*,\theta})$  respectively, are generated in order evaluate  
 239 the sand transport rate  $Q$  within MC approach.  $u_{*t}$  and  $u_{*,\theta}$  cardinality  $\# = 1e+6$  is adopted for each direction. Sand  
 240 transport rate results are organized in the form of sand rose in Figure 6(a) in analogy with the wind rose in Figure  
 241 5(a). In fact, the length of each bin is the same in both roses. The wind rose and the sand rose have the same di-  
 242 rection frequencies. Hence, the relative length of each bin is the same in both roses. This is due to the fact that one

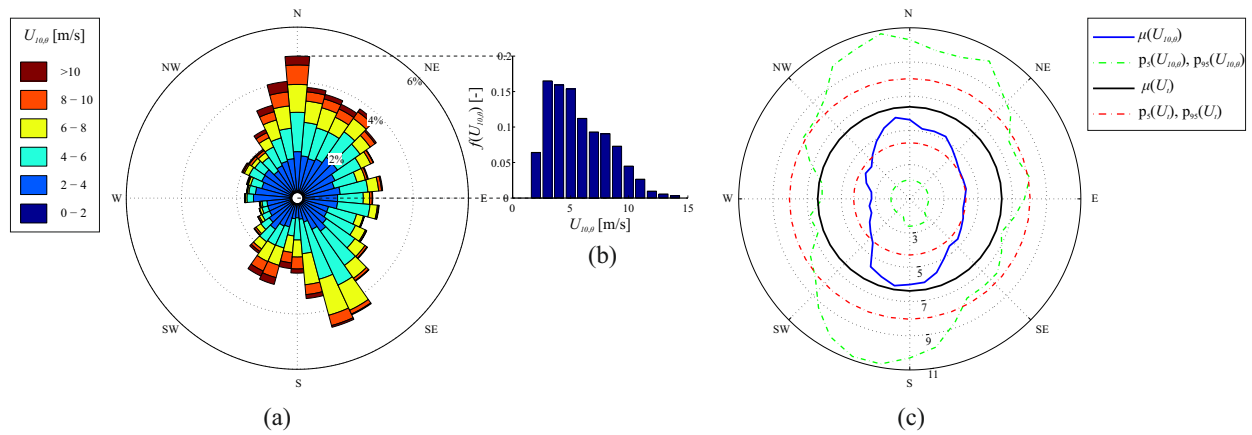


Figure 5: Site 1. Directional statistics of mean wind speed: wind rose (a), empirical probability density function of the wind speed in North direction (b), polar diagram of  $U_{10}$  and  $U_t$  statistics (c)

243 realization of  $Q$  for a given direction results from the corresponding realization of  $U_{10}$  along the same direction  $\theta$ .  
 244 Conversely, the probability density function  $f(Q_\theta)$  for each direction does not result from a simple rescaling of the  
 245 corresponding  $f(u_{*,\theta})$ , because of the piece-wise, non-linear transformation (Eq. 1). In particular, for  $0 < u_{*,\theta} < u_{*t}$ ,  
 246  $Q_\theta = 0$  even if this does not correspond to wind calm conditions. Hence, the color pattern in each bin significantly  
 247 varies. An example is explicitly given by the empirical probability density functions for North direction (Fig. 5-b and  
 248 6-b). Figure 6(c) depicts the mean value and the 95<sup>th</sup> percentile of the sand transport rate as a function of  $\theta$ .  $\mu(Q_\theta)$   
 249 and  $p_{95}(Q_\theta)$  are higher for winds blowing from around North and from South-SouthWest, that are the direction for which  
 $p_{95}(U_{10,\theta}) > p_{95}(U_t)$  (see Fig.5-c).

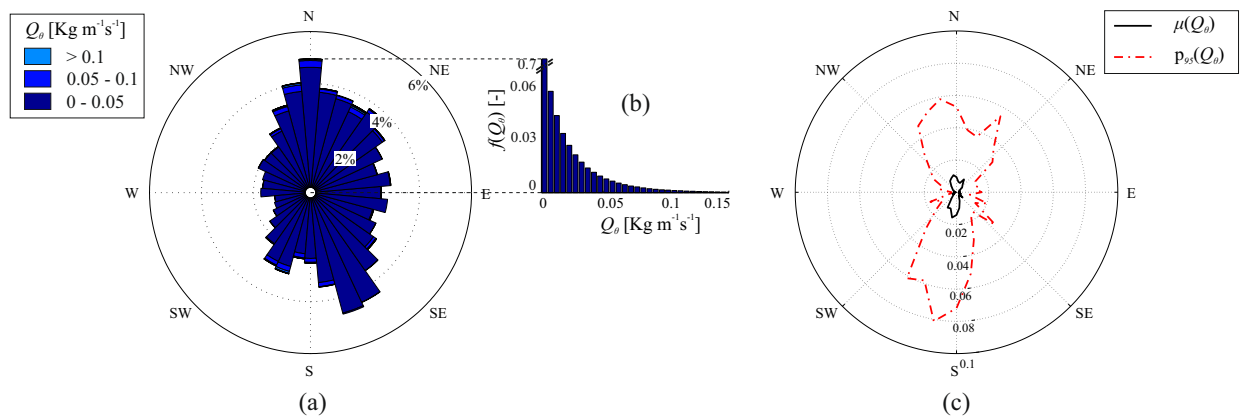


Figure 6: Site 1. Sand transport rate statistics: sand transport rate rose (a), sand transport rate empirical probability density function in North direction (b), polar diagram of sand transport rate statistics (c)

250  
 251 The following remarks can be outlined. First, the distribution is no longer a continuous distribution: its hybrid nature  
 252 is due to the first part of the piece-wise transformation, i.e.  $Q_\theta = 0$  if  $u_{*,\theta} \leq u_{*t}$ . Second, the distribution is no longer  
 253 a Weibull-type one, due to the non-linear transformation. In particular, distributions are strongly right-sided skewed.  
 254 Finally, the sand transport rate directional statistics are strongly bimodal, with North and South prevailing directions,  
 255 in contrast with the very broad wind directionality (Fig.5-a). This is due to the fact that the sand transport rate  $Q_\theta$   
 256 depends on the cube of the effective shear velocity  $u_{*,\theta,eff}^3 = u_{*,\theta}^3 - u_{*,\theta}^2 u_{*t}$ . Referring to Figure 5(c), low-speed winds  
 257 from West and East do not contribute to  $Q_\theta$ , while high-speed winds from North and South almost solely contribute

258 to  $Q_\theta$ .

259 The drift potential over the sampling interval  $D_{\theta,\Delta t}$  [ $m^3 m^{-1} hr^{-1}$ ] is simply obtained from  $Q_\theta$  [ $Kg m^{-1} s^{-1}$ ] consid-  
 260 ering the packed bulk sand density  $\rho_b = 1.8e+3 kg m^{-3}$ .

261 The number of occurrences  $N_\theta$  is assessed by bootstrapping a sample of cardinality  $N = 8768$  (i.e. the number of  $\Delta t$   
 262 in  $T$ ) from the actual wind velocity dataset. The wind direction frequencies  $N_\theta/N$  are shown by box plots in Figure  
 263 7(a). On the same graph, calm wind frequency is plotted too. It should be highlighted that the influence of calm wind  
 264 on  $D_\theta$  is taken into account by  $N_\theta$ . In fact, wind direction frequencies are computed considering the frequency of calm  
 265 wind (see Eq.3).

266 Once  $D_{\theta,\Delta t}$  and  $N_\theta$  are assessed over each direction, the drift potentials  $D_\theta$  over  $T = 1$  year are obtained following  
 267 Equation 9. In particular, Equation 9 is applied by bootstrapping a sample of  $D_{\theta,\Delta t}$  and  $N_\theta$  realizations, both having  
 268 cardinality  $\# = 1e+5$ . The same cardinality  $\#_{D_\theta}$  for each  $D_\theta$  follows from MC. In Figure 7(b), drift potential mean  
 269 values and percentiles are plotted as a function of  $\theta$  to summarize directional statistics and related  $f(D_\theta)$ . The non-  
 270 parametric probability density function  $f(D_\theta)$  which describes the incoming sand drift from North in  $T = 1$  year, is  
 shown in Figure 7(c) by way of example.

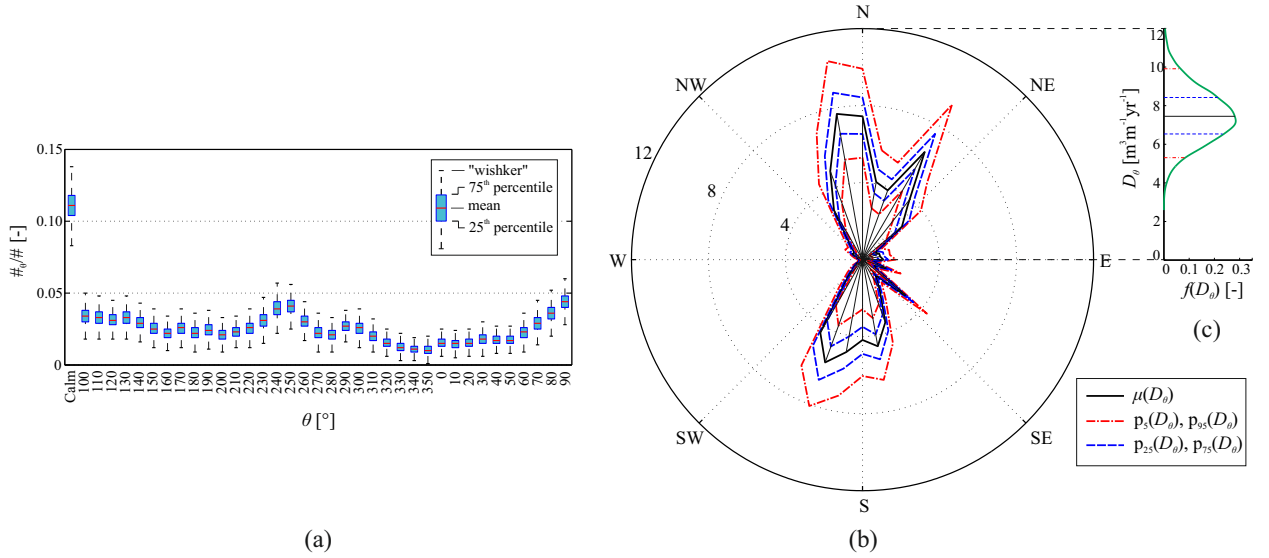


Figure 7: Site 1. Wind direction frequencies by  $N_\theta/N$  box plot (a). Drift potential  $D_\theta$  directional statistics (b), drift potential probability density function in North direction (c).

271 Three remarks follow. First,  $N_\theta$  variability is low, at least for this site. Hence, the variance of  $D_\theta$  is mainly due to  
 272 the variance of  $D_{\theta,\Delta t}$ , while the variance of  $N_\theta$  is relatively small (see Eq.8). Second, the drift potential directional  
 273 statistics are strongly bimodal with North and South prevailing directions in accordance with the sand transport rate  
 274 ones (see Fig.6-c). Finally, the cumulative sum of the very skewed  $f(Q_\theta)$  gives rise to almost symmetric  $f(D_\theta)$ . This  
 275 is compliant to the central limit theorem: the sum of independent random variables tends to a normally distributed  
 276 random variable even if the original random variables are not.

277 Figure 8 provides a synopsis of the uncertainty propagation from erosion threshold and wind speed to sand trans-  
 278 port rate and drift potential. The coefficient of variation and skewness modulus of these random variables are plot-  
 279 ted as a function of the direction  $\theta$  in Figures 8 (a) and (b), respectively. The *c.o.v.* of the input random variables  
 280 ( $U_{10,\theta}$ ,  $U_t$ ) is relatively small (*c.o.v.*  $\approx 1e-0.5$ ). Uncertainty is magnified by an order of magnitude proceeding to  
 281  $Q_\theta$  (*c.o.v.*  $\approx 1e+0.5$ ), while *c.o.v.* is damped again passing from  $Q_\theta$  to  $D_\theta$  (*c.o.v.*  $\approx 1e-0.5$ ). Indeed, on the one  
 282 hand, transformation of random variables done in order to assess  $Q$  (i.e. Eq.1) magnifies the uncertainty of the initial  
 283 random variables  $U_{10,\theta}$  and  $U_t$ . On the other hand, the random sum of identically and independent distributed random  
 284 variables (Eq.9) damps *c.o.v.* The *c.o.v.* of the random variables above shows slight differences over  $\theta$ .  $U_t$  does not  
 285 depend on  $\theta$  at all, *c.o.v.* ( $U_{10,\theta}$ ) is almost constant for this site, *c.o.v.* ( $Q_\theta$ ) and *c.o.v.* ( $D_\theta$ ) in turn are higher for winds  
 286

287 blowing from East and West, i.e. the less frequent wind directions. The skewness modulus shows approximately the  
 288 same behavior of *c.o.v.*  $|sk(Q_\theta)|$  increases significantly with respect to  $|sk(U_i)|$  and  $|sk(U_{10,\theta})|$ , while  $|sk(D_\theta)|$  decreases  
 again. In particular,  $|sk(D_\theta)|$  is lower for winds blowing from around North and South directions.

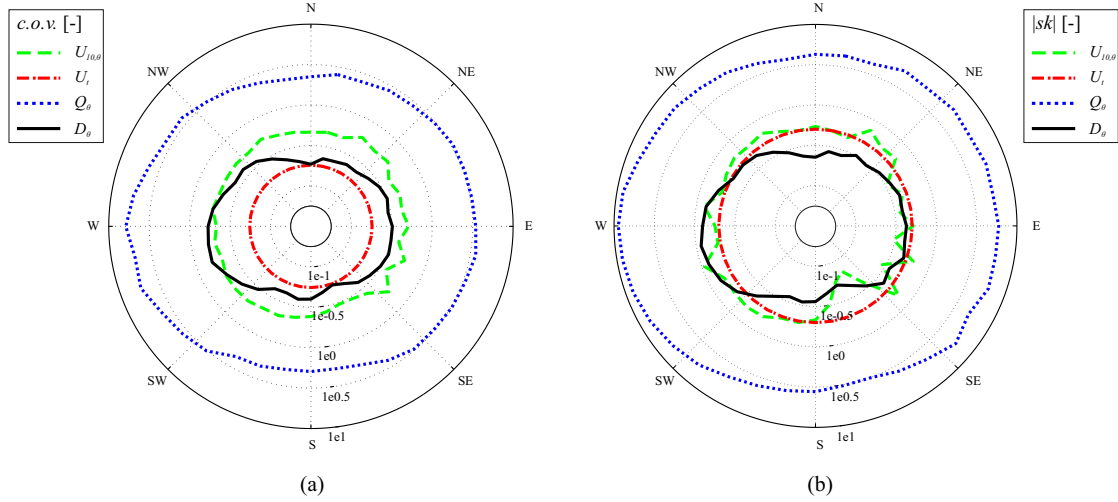


Figure 8: Site 1. Uncertainty propagation from  $U_{10}$  and  $U_i$  to  $Q_\theta$  and  $D_\theta$  in terms of polar diagrams of coefficient of variation (a) and skewness (b)

289 Finally, in Figure 9(a), each black dot represents a single realization the resultant drift potential  $R$ . The radial  
 290 coordinate of the dots is the vector magnitude  $|R|$ , while the angular coordinate is the vector direction  $\hat{R}$ . Each realization  
 291 of  $R$  is numerically obtained from one realization of  $D$  through Equations 4 and 9 by bootstrapping (Efron  
 292 and Tibshirani, 1993). The ensemble of black dots graphically visualizes the whole set of numerical realizations of  $R$ .  
 293 The cardinality of  $R$  is  $\#_R = 5e+4$ . In the following we call "realization cloud" the ensemble of black dots. The mean  
 294 resultant drift potential vector  $\mu(R)$  is depicted by the red arrow on the same graph.  $R$  can be described in probabilistic  
 295 terms by the joint probability density function  $f(|R|, \hat{R})$  of the two random variables  $|R|$  and  $\hat{R}$ .  $f(|R|)$  and  $f(\hat{R})$  marginal  
 296 densities are shown in Figure 9(b) and (c), respectively.

297 The realization cloud appears to be comma-shaped in circular coordinates, i.e. tear-shaped in cartesian coordinates.  
 298 This shape indicates a significant skewness of  $\hat{R}$ , as testified by its marginal distribution. The radial width of the  
 299 realization cloud provides a qualitative graphical reading of the variability of  $R$  magnitude. The circumferential extent  
 300 of the cloud qualitatively describe the variability of  $R$  direction. For this site, the variability of  $\hat{R}$  is by far higher than  
 301 the one of  $|R|$ . This is confirmed by the marginal distributions in Figures 9(b) and (c). From a qualitative point of  
 302 view, it is worth pointing out that the only mean value (red arrow) is a poor description of the sand drift phenomenon.  
 303 Conversely, realization cloud and related high-order statistics provide a more complete description. In general, SD-  
 304 WA approach loses fundamental information of  $R$ , while the proposed SWP approach provides complete statistics.  
 305 The quantitative statistics of  $R$  for this Site and all remaining Sites are reported in the following Subsection.

### 307 3.3. Comparative analysis Sites 1-5

308 In the following, all the selected Sites are accounted for. Both wind and windblown sand fields are probabilisti-  
 309 cally evaluated and critically compared.

310 In Figure 10,  $U_{10}$  wind roses and polar diagrams of resultant drift potential  $R$  are represented on Arabian Peninsula  
 311 map. Realization clouds of the resultant drift potential and marginal densities are plotted as well. On the same graphs,  
 312 the mean values of  $R$  are reported (red arrows). In short, Figure 10 collects the results of the initial and final step of the  
 313 proposed procedure. Wind rose shape testifies a variety of wind regimes: wide unimodal, i.e. Site 2, acute bimodal,  
 314 i.e. Site 3, obtuse bimodal, i.e. Sites 1 and 5, complex, Site 4. Realization cloud shape, dimension and density change  
 315 significantly moving from a site to another. The realization clouds appear to be comma-shaped in polar diagrams  
 316 (i.e. tear-shaped in cartesian coordinates), or kidney-shaped (i.e. elliptical-shaped in cartesian coordinates). Comma

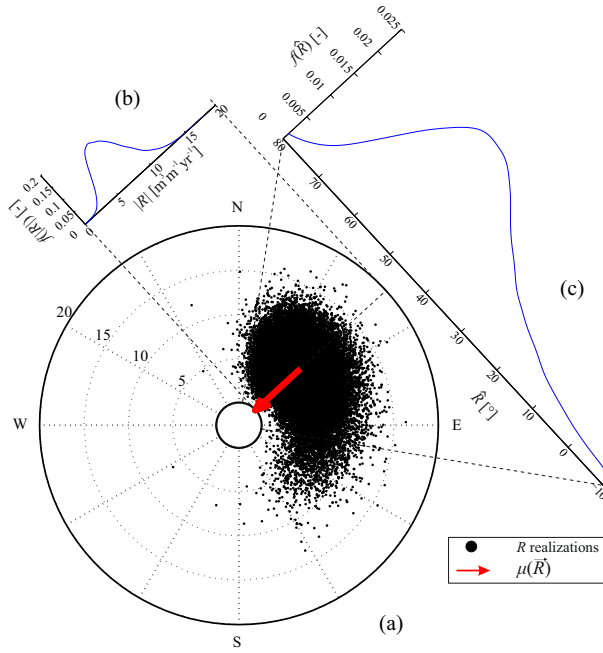


Figure 9: Site 1. Resultant drift potential (a), resultant drift potential magnitude marginal density (b) and resultant drift potential direction marginal density (c).

317 shape (Sites 1 and 5) indicates a significant skewness of  $\hat{R}$ , while kidney shape (Sites 2,3,4) indicates weakly skewed  
 318 magnitude and direction. The wider the realization cloud in radial and/or circumferential direction, the higher the  
 319 variation of  $R$ , in magnitude and direction, respectively. Variations of both  $|R|$  and  $\hat{R}$  are small at Sites 2 and 3, so  
 320 that kidney-shaped cloud appear as elliptical. Site 4 is remarkably characterized by very high variation of  $\hat{R}$  and a  
 321 small variation of  $|R|$ . The marginal densities  $f(|R|)$  and  $f(\hat{R})$  clearly reflect these differences. In particular, while in  
 322 some cases they recall Gaussian distributions (Sites 2 and 3), in others they appear asymmetric, mainly with respect  
 323 to the direction ( $f(\hat{R})$  at Sites 1 and 5). In general, the relation between wind rose and realization cloud is not straight-  
 324 forward, because of the non-linear relation between  $U_{10}$  and  $Q$ . Furthermore, wind roses graphically point out wind  
 325 direction frequencies much more effectively than wind speed frequencies. However, it is worth pointing out that the  
 326 more complex the wind rose, the wider the realization cloud.

327 Non-dimensional statistics of both  $|R|$  and  $\hat{R}$  are reported in Table 3 to summarize the obtained results and quan-  
 328 titatively compare the Sites. Variation and skewness of  $|R|$  and  $\hat{R}$  are assessed in order to understand how much the  
 329 random variables are dispersed and how far are from Gaussianity. The variability of  $|R|$  is expressed by means of  
 330 *c.o.v.*, while the variability of  $\hat{R}$  is directly expressed by the angular deviation  $\sigma$ . It is worth to point out that since  $\hat{R}$   
 331 is a circular random variable, circular statistics is assessed (Fisher, 1995; Berens, 2009). The lowest variability is ad-  
 332 dressed to Site 2, i.e. the Site with unimodal wind regime, while the highest variability is addressed to e.g. Sites 1 and  
 333 4, i.e. the Sites with obtuse bimodal or complex wind regimes. Concerning probability density functions symmetry,  
 334 Sites 1 and 5 show the most skewed distributions, while Site 3 one is almost symmetric.

335 The design of infrastructures in arid environments should be based on sand drift magnitude related to a low prob-  
 336 ability of exceedance. Hence, characteristic values (i.e. extreme percentiles) of both  $R$  magnitude and direction are  
 337 included in Table 3. The ratio between 95<sup>th</sup> percentile and mean value  $p_{95}/\mu$  is assessed as regards  $R$  magnitude. The  
 338 study gives rise to characteristic values up to  $\approx 1.6$  times the mean value (Site 1). In other words, the evaluation of  
 339  $|R|$  in mean terms only significantly underestimates the amount of transported sand. The angular distance  $|p_{95} - p_5|$  is  
 340 evaluated, regarding  $\hat{R}$ . Both percentiles are referred to anti-clockwise circular direction from East. In other words,  
 341  $|p_{95} - p_5|$  provides a quantitative measure of the variability of  $\hat{R}$  based on characteristics directions. This measure is the  
 342 well posed probabilistic reading of the estimate of drift direction variability proposed by Fryberger and Dean (1979)

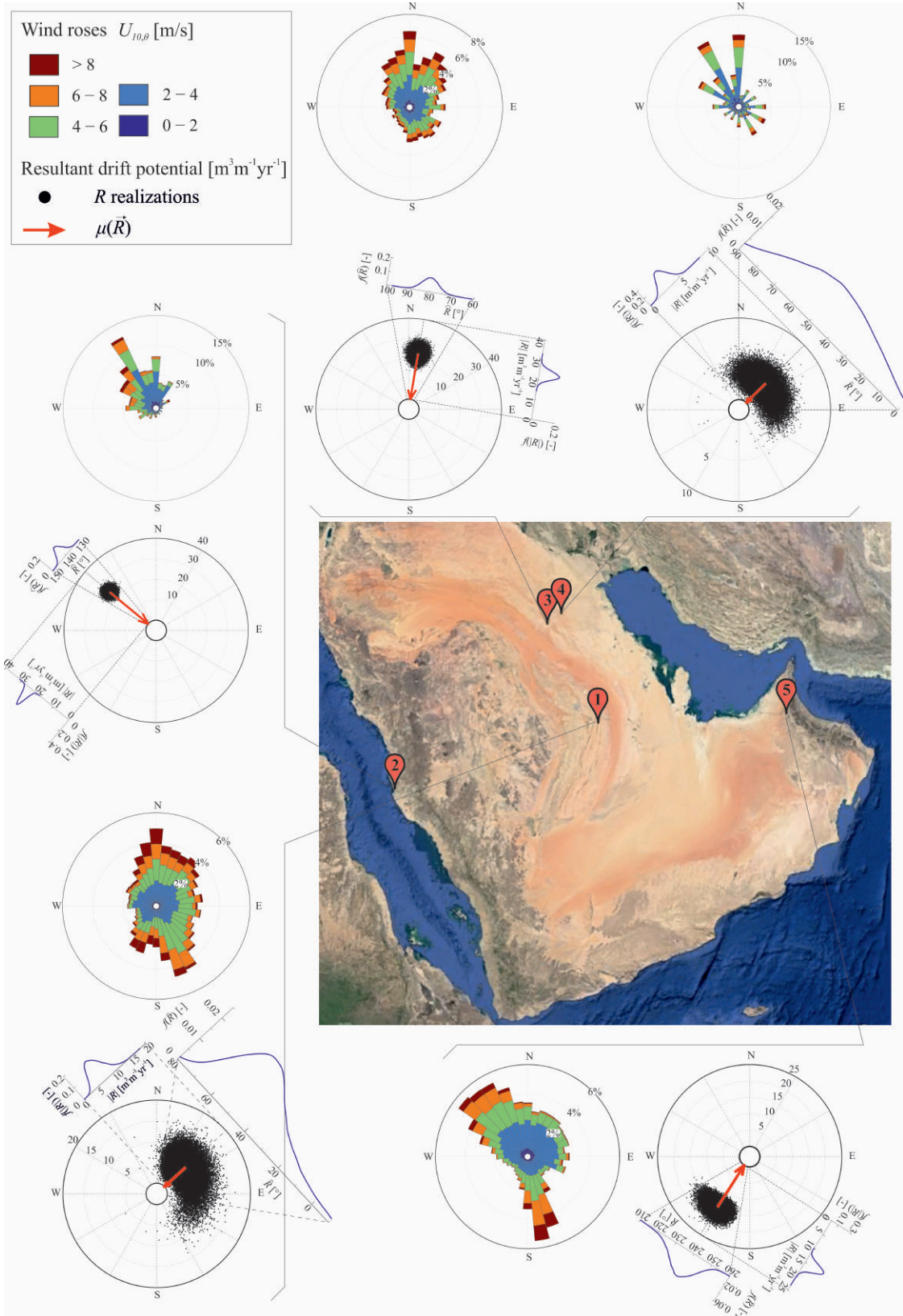


Figure 10: Sites 1-5. Wind roses and resultant drift potentials around Arabian Peninsula

343 in deterministic terms through Equation 5. The highest  $|p_{95} - p_5|$  angular distance is observed for Site 4, i.e.  $\approx 88^\circ$ ,  
 344 while the lowest,  $\approx 8^\circ$ , is observed for Site 2.

Table 3: Sites 1-5. Statistics of resultant drift potential magnitude and direction

	$ R  [m^3 m^{-1} yr^{-1}]$			$\hat{R} [^\circ]$		
	<i>c.o.v.</i> [-]	<i>sk</i> [-]	$p_{95}/\mu$ [-]	$\sigma$ [°]	<i>sk</i> [-]	$ p_{95} - p_5  [^\circ]$
Site 1	0.32	0.37	1.57	20.77	2.61	77.22
Site 2	0.06	0.02	1.09	2.52	0.38	8.28
Site 3	0.10	0.01	1.16	3.88	-0.05	12.78
Site 4	0.27	0.11	1.46	24.09	0.60	87.80
Site 5	0.10	0.28	1.17	7.11	1.05	23.22

344

#### 345 4. Conclusions

346 The present study introduces a new Sand-Wind Probabilistic (SWP) approach to evaluate incoming windblown  
 347 sand drift potentials and resultant drift potentials. The approach adapts the general framework proposed by [Fryberger  
 348 and Dean \(1979\)](#) in order to deal with the sources of uncertainty related to both wind and sand subfields. The input  
 349 uncertainties on  $U_{10}$  and  $u_{*t}$  propagate to the final result, i.e.  $R$ , passing through the definition of  $Q_\theta$  and  $D_\theta$ .

350 The following concluding remarks can be outlined, bearing in mind the three kickoff questions raised in Intro-  
 351 duction. First, uncertainty of both threshold shear velocity and mean wind velocity are magnified passing to the  
 352 directional sand transport rate  $Q_\theta$  by about an order of magnitude. Subsequently, uncertainty is damped from  $Q_\theta$   
 353 to the drift potential  $D_\theta$ , and it is further damped to the resultant drift  $R$ . Magnification is due to the cubic dependency  
 354 of  $Q$  versus  $u_*$  and  $u_{*t}$ , while damping results from cumulating in time and vector summing over directions. Second,  
 355 the probability distribution of the resultant drift potential changes significantly from a site to another in the same  
 356 region. Complex wind regimes are particularly prone to cause windblown sand drift with high inborn variability. For  
 357 instance, the highest *c.o.v.*( $|R|$ ) and  $\sigma(\hat{R})$  are referred to sites showing obtuse bimodal or complex wind roses. Changes  
 358 in the sand granulometry and related shear threshold velocity probability distribution from one site to another also  
 359 affect  $R$ . Finally, the proposed SWP probabilistic approach allows to obtain characteristic values of  $R$ , while the Sand  
 360 Deterministic-Wind Averaged (SD-WA) approach adopted up to now in scientific literature and engineering practice  
 361 does not provide sufficient statistics to describe correctly the phenomenon. The gap between characteristic and mean  
 362 value of RDP makes the approach of interest for engineering practice and grounds the semi-probabilistic approach  
 363 to design of civil infrastructure in arid regions. Regarding sites with complex wind regimes, on the one hand, the  
 364 characteristic value of  $|R|$  is about 1.5 times the mean value. On the other hand, the angular distance between the mean  
 365 direction and the characteristic values of  $\hat{R}$  is about  $40^\circ$ .

366 In the light of the obtained results, we suggest four research perspectives. First, the role played by each considered  
 367 random variable in variability of sand drift should be ascertained by means of a numerical sensitivity study, i.e. by  
 368 setting a constant grain diameter (and hence the probability density function of  $u_{*t}$ ) and varying the wind field, and  
 369 vice versa. Second, the proposed approach needs to be validated by in-situ, long-term, continuous and automatic  
 370 recording of the sand drift, analogously to wind speed measurements. Traditional sand trap ([Nickling and Neuman,  
 371 1997; Weaver and Wiggs, 2011](#)) are not adequate to this purpose. Piezoelectric sand flux sensor ([Udo, 2009](#)) proved  
 372 encouraging performances during prototype testing in operational conditions. This technology will enable in the next  
 373 future years-long site measurements. Third, having in mind the vast amount of sand transport rate models in litera-  
 374 ture,  $Q$  model uncertainty should be investigated and, if significant, incorporated in the adopted probabilistic method.  
 375 Finally, sand drift extreme values statistics would worth to be described in order to assess how much stand storms  
 376 weigh on the total amount of the resultant drift potential and on disastrous events.

## 377 Acknowledgments

378 The study has been developed in the framework of the Windblown Sand Modeling and Mitigation joint research,  
379 development and consulting group established between Politecnico di Torino and Optiflow Company. The research  
380 activity of Luca Bruno and Davide Fransos has been developed within the MSCA-ITN-2016-EID SMaRT research  
381 project. This project has received funding from the European Union's Horizon 2020 research and innovation pro-  
382 gramme under grant agreement No 721798. The authors wish to thank Luigi Preziosi, member of the WSMM group,  
383 and Maria Pia Repetto, Università di Genova, for the stimulating discussions about the topics of the paper.

## 384 References

- 385 Al-Awadhi, J.M., Al-Awadhi, A.A., 2009. Modeling the aeolian sand transport for the desert of Kuwait: Constraints by field observations. *Journal*  
386 *of Arid Environments* 73, 987–995. doi:10.1016/j.jaridenv.2009.04.023.
- 387 Al-Harthi, A., 2002. Geohazard assessment of sand dunes between Jeddah and Al-Lith, western Saudi Arabia. *Environmental Geology* 42,  
388 360–369. doi:10.1007/s00254-001-0501-z.
- 389 Al-Sari, A., Uddin, W., 1981. Eolian sand problem: an engineering evaluation, in: *Proceedings Symposium Geotechnical Problems in Saudi*  
390 *Arabia*.
- 391 Alghamdi, A.A., Al-Kahtani, N.S., 2005. Sand Control Measures and Sand Drift Fences. *J. Perform. Constr. Facil.* 19, 295–299. doi:10.1061/  
392 (ASCE)0887-3828(2005)19:4(295).
- 393 Bagnold, R., 1941. *The Physics of Blown Sand and Desert Dunes*. Methuen. doi:10.1007/978-94-009-5682-7.
- 394 Barchyn, T.E., Hugenholtz, C.H., 2011. Comparison of four methods to calculate aeolian sediment transport threshold from field data: Implications  
395 for transport prediction and discussion of method evolution. *Geomorphology* 129, 190–203. doi:10.1016/j.geomorph.2011.01.022.
- 396 Barchyn, T.E., Martin, R.L., Kok, J.F., Hugenholtz, C.H., 2014. Fundamental mismatches between measurements and models in aeolian sediment  
397 transport prediction: The role of small-scale variability. *Aeolian Research* 15, 245–251. doi:10.1016/j.aeolia.2014.07.002.
- 398 Berens, P., 2009. Cirstat: A matlab toolbox for circular statistics. *Journal of Statistical Software* 31. doi:10.18637/jss.v031.i10.
- 399 Bofah, K.K., Al-Hinai, K.G., 1986. Field tests of porous fences in the regime of sand-laden wind. *Journal of Wind Engineering and Industrial*  
400 *Aerodynamics* 23, 309–319. doi:10.1016/0167-6105(86)90051-6.
- 401 Bogle, R., Redsteer, M., Vogel, J., 2015. Field measurement and analysis of climatic factors affecting dune mobility near Grand Falls on the Navajo  
402 Nation, southwestern United States. *Geomorphology* 228, 41–51. doi:10.1016/j.geomorph.2014.08.023.
- 403 Burlando, M., De Gaetano, P., Pizzo, M., Repetto, M., Solari, G., Tizzi, M., 2013. Wind climate analysis in complex terrain. *Journal of Wind*  
404 *Engineering and Industrial Aerodynamics* 123, 349–362. doi:10.1016/j.jweia.2013.09.016.
- 405 Caffisch, R., 1998. Monte carlo and quasi-monte carlo methods. *Acta Numerica* 7, 1–49. doi:10.1017/S096249290002804.
- 406 Carta, J.A., Ramírez, P., Velázquez, S., 2009. A review of wind speed probability distributions used in wind energy analysis: Case studies in the  
407 Canary Islands. *Renewable and Sustainable Energy Reviews* 13, 933–955. doi:10.1016/j.rser.2008.05.005.
- 408 Cheng, J., Xue, C., 2014. The sand-damage-prevention engineering system for the railway in the desert region of the Qinghai-Tibet plateau. *J.*  
409 *Wind Eng. Ind. Aerodyn.* 125, 30–37. doi:10.1016/j.jweia.2013.11.016.
- 410 Cheng, J.J., Jiang, F.Q., Xue, C.X., Xin, G.W., Li, K.C., Yang, Y.H., 2015. Characteristics of the disastrous wind-sand environment along railways in  
411 the Gobi area of Xinjiang, China. *Atmospheric Environment* 102, 344–354. doi:10.1016/j.atmosenv.2014.12.018.
- 412 Dong, Z., Chen, G., He, X., Han, Z., Wang, X., 2004. Controlling blown sand along the highway crossing the Taklimakan Desert. *Journal of Arid*  
413 *Environments* 57, 329–344. doi:10.1016/j.jaridenv.2002.02.001.
- 414 Dong, Z., Liu, X., Wang, H., Wang, X., 2003. Aeolian sand transport: a wind tunnel model. *Sediment. Geol.* 161, 71–83. doi:10.1016/  
415 S0037-0738(03)00396-2.
- 416 Duan, S., Cheng, N., Xie, L., 2013. A new statistical model for threshold friction velocity of sand particle motion. *Catena* 104, 32–38. doi:10.  
417 1016/j.catena.2012.04.009.
- 418 Edgell, H.S., 2006. *Arabian Desert*. Springer.
- 419 Edwards, B.L., Namikas, S.L., 2015. Characterizing the sediment bed in terms of resistance to motion: Toward an improved model of saltation  
420 thresholds for aeolian transport. *Aeolian Research* 19, 123–128. doi:10.1016/j.aeolia.2015.10.004.
- 421 Efron, B., Tibshirani, R., 1993. *An Introduction to the Bootstrap*. Chapman & Hall/CRC, New York.
- 422 Ehlen, J., 1993. *Physical Characteristics of Some Solis from the Middle East*. Technical Report. U.S. Army Topographic Engineering Center  
423 (TEC-0032).
- 424 Fisher, N., 1995. *Statistical Analysis of Circular Data*. Cambridge University Press. doi:https://doi.org/10.1017/CB09780511564345.
- 425 Fryberger, S., Dean, G., 1979. A Study of Global Sand Seas. chapter Dune forms and wind regime. pp. 137–155.
- 426 Hoonhout, B.M., de Vries, S., 2016. A process-based model for aeolian sediment transport and spatiotemporal varying sediment availability.  
427 *Journal of Geophysical Research: Earth Surface* 121, 1555–1575. doi:10.1002/2015JF003692.
- 428 Iversen, J., White, B., 1982. Saltation threshold on earth, mars and venus. *Sedimentology* 29, 111–119. doi:10.1111/j.1365-3091.1982.  
429 tb01713.x.
- 430 Kilibarda, Z., Kilibarda, V., 2016. Seasonal geomorphic processes and rates of sand movement at Mount Baldy dune in Indiana, USA. *Aeolian*  
431 *Research* 23A, 103–114. doi:10.1016/j.aeolia.2016.10.004.
- 432 Kok, J.F., Parteli, E.J.R., Michaels, T.I., Karam, D.B., 2012. The physics of wind-blown sand and dust. *Reports on Progress in Physics* 75, 106901.  
433 doi:10.1088/0034-4885/75/10/106901.
- 434 Lancaster, N., Baas, A., 1998. Influence of vegetation cover on sand transport by wind: field studies at Owens Lake, California. *Earth Surface*  
435 *Processes and Landforms* 23, 69–82. doi:10.1002/(SICI)1096-9837(199801)23:1<69::AID-ESP823>3.0.CO;2-G.

- 436 Lettau, K., Lettau, H., 1978. Experimental and micro-meteorological field studies of dune migration. Technical Report 101, 110-147. Exploring  
437 the Worlds Driest Climate (IES Report, 101, 110147).
- 438 Liu, L., Yang, Y., Shi, P., Zhang, G., Qu, Z., 2015. The role of maximum wind speed in sand-transporting events. *Geomorphology* 238, 177–186.  
439 doi:10.1016/j.geomorph.2015.03.007.
- 440 McKenna, N., 2003. Effects of temperature and humidity upon the entrainment of sedimentary particles by wind. *Boundary Layer Meteorol.* 108,  
441 61–89. doi:10.1023/A:1023035201953.
- 442 McKenna Neuman, C., Nickling, W., 1989. A theoretical and wind tunnel investigation of the effect of capillary water on the entrainment of  
443 sediment by wind. *Can. J. Soil Sci.* 69, 79–96. doi:10.4141/cjsss89-008.
- 444 Middleton, N., Sternberg, T., 2013. Climate hazards in drylands: A review. *Earth-Sci. Rev.* 126, 48–57. doi:10.1016/j.earscirev.2013.07.  
445 008.
- 446 Nickling, W.G., 1988. The initiation of particle movement by wind. *Sedimentology* 35, 499–511. doi:10.1111/j.1365-3091.1988.tb01000.x.
- 447 Nickling, W.G., Neuman, C.M., 1997. Wind tunnel evaluation of a wedge-shaped aeolian sediment trap. *Geomorphology* 18, 333. doi:10.1016/  
448 S0169-555X(96)00040-2.
- 449 Pye, K., Tsoar, H., 2009. *Aeolian Sand and Sand Dunes*. Springer. doi:10.1007/978-3-540-85910-9.
- 450 Raffaele, L., Bruno, L., Pellerey, F., Preziosi, L., 2016. Windblown sand saltation: A statistical approach to fluid threshold shear velocity. *Aeolian*  
451 *Research* 23, 79–91. doi:10.1016/j.aeolia.2016.10.002.
- 452 Redding, J.H., Lord, J.A., 1981. Designing for the effects of windblown sand along the new Jessah-Riyadh-Dammam expressway, in: *Symposium*  
453 *on Geotechnical Problems in Saudi Arabia*, pp. 363–395.
- 454 Repetto, M., Solari, G., 2004. Directional wind-induced fatigue of slender vertical structures. *Journal of Structural Engineering* 130, 1032–1040.  
455 doi:10.1061/~ASCE!0733-9445~2004!130:7~1032!
- 456 Riksen, M.J., Goossens, D., Huiskes, H., Krol, J., Slim, P., 2016. Constructing notches in foredunes: Effect on sediment dynamics in the dune  
457 hinterland. *Geomorphology* 15, 340–352. doi:10.1016/j.geomorph.2015.10.021.
- 458 Rizvi, A., 1989. Planning responses to aeolian hazards in arid regions. *Journal of King Saud University, Architecture & Planning* 1, 59–74.
- 459 Shao, Y., 2008. *Physics and Modelling of Wind Erosion*. Springer. doi:10.1007/978-1-4020-8895-7.
- 460 Shao, Y., Lu, H., 2000. A simple expression for wind erosion threshold friction velocity. *J. Geophys. Res.* 105, 22437–43. doi:10.1029/  
461 2000JD900304.
- 462 Sherman, D.J., Bailiang, L., Ellis, J.T., Farrell, E.J., Maia, L., Granja, H., 2013. Recalibrating aeolian sand transport models. *Earth Surf. Process.*  
463 *Landforms* 38, 169–178. doi:10.1002/esp.3310.
- 464 Sherman, D.J., Li, B., 2012. Predicting aeolian sand transport rates: A reevaluation of models. *Aeolian Research* 3, 371–378. doi:10.1016/j.  
465 aeolia.2011.06.002.
- 466 Stipho, A.S., 1992. Aeolian sand hazards and engineering design for desert regions. *Quarterly Journal of Engineering Geology* 25, 83–92.  
467 doi:10.1144/GSL.QJEG.1992.025.02.02.
- 468 Takle, E., Brown, J., 1978. Note on the use of weibull statistics to characterize wind-speed data. *J. Appl. Meteorol.* 17, 556–559. doi:10.1175/  
469 1520-0450(1978)017<0556:NOTUOW>2.0.CO;2.
- 470 Udo, K., 2009. New method for estimation of aeolian sand transport rate using ceramic sand flux sensor (ud-101). *Sensors* 9, 9058–9072.  
471 doi:10.3390/s91109058.
- 472 del Valle, H., Rostagno, C., Coronato, F., Bouza, P., Blanco, P., 2008. Sand dune activity in north-eastern Patagonia. *Journal of Arid Environments*  
473 72, 411–422. doi:10.1016/j.jaridenv.2007.07.011.
- 474 Wang, X.M., Zhang, C.X., Hasi, E., Dong, Z.B., 2010. Has the Three Norths Forest Shelterbelt Program solved the desertification and dust storm  
475 problems in arid and semiarid China? *Journal of Arid Environments* 74, 13–22. doi:10.1016/j.jaridenv.2009.08.001.
- 476 Weaver, C.M., Wiggs, G.F.S., 2011. Field measurements of mean and turbulent airflow over a barchan sand dune. *Geomorphology* 128, 32–41.  
477 doi:10.1016/j.geomorph.2010.12.020.
- 478 Yang, X., Forman, S., Hu, F., Zhang, D., Liu, Z., Li, H., 2016. Initial insights into the age and origin of the Kubuqi sand sea of northern China.  
479 *Geomorphology* 259, 30–39. doi:10.1016/j.geomorph.2016.02.004.
- 480 Yang, Y., Qu, Z., Shi, P., Liu, L., Zhang, G., Tang, Y., Hu, X., Lv, Y., Xiong, Y., Wang, J., Shen, L., Lv, L., Sun, S., 2014. Wind regime and  
481 sand transport in the corridor between the Badain Jaran and Tengger deserts, central Alxa Plateau, China. *Aeolian Research* 12, 143–156.  
482 doi:10.1016/j.aeolia.2013.12.006.
- 483 Zakeri, J.A., 2012. Investigation on railway track maintenance in sandy-dry areas. *Structure and Infrastructure Engineering: Maintenance,*  
484 *Management, Life-Cycle Design and Performance* 8, 135–140. doi:10.1080/15732470903384921.
- 485 Zhang, C., Zou, X., Cheng, H., Yang, S., Pan, X., Liu, Y., Dong, G., 2007. Engineering measures to control windblown sand in shiquanhe town,  
486 tibet. *J. Wind Eng. Ind. Aerod.* 95, 53–70. doi:10.1016/j.jweia.2006.05.006.
- 487 Zhang, K.c., Qu, J.j., Liao, K.t., Niu, Q.h., Han, Q.j., 2010. Damage by wind-blown sand and its control along Qinghai-Tibet Railway in China.  
488 *Aeolian Research* 1, 143–146. doi:10.1016/j.aeolia.2009.10.001.
- 489 Zio, E., Pedroni, N., 2013. Literature review of methods for representing uncertainty. *Foundation for an Industrial Safety Culture*.